Clim Dyn (2016) 46:2759–2771
DOI 10.1007/s00382-015-2729-4

The zonal movement of the Indian–East Asian summer monsoon interface in relation to the land–sea thermal contrast anomaly over East Asia

Yun Tao[1,2,3] · Jie Cao[2,3] · Guangdong Lan[4] · Qin Su[2]

Received: 18 January 2015 / Accepted: 23 June 2015 / Published online: 7 July 2015

Abstract Based on atmospheric circulation reanalysis, global gridded precipitation, and outgoing longwave radiation datasets, this study reveals the physical process through which the land–sea thermal contrast over East Asia interrelates with the variability of the interface between the Indian summer monsoon and East Asian summer monsoon (IIE). The results indicate that the release of latent heating exerted by the low-frequency variability of anomalous land–sea thermal contrast is one of the most important physical processes correlating with the zonal movement of the IIE, in which the release of latent heating over eastern East Asia makes the greatest contribution. When a lower apparent moisture sink occurs over the South China Sea but a higher one over southern China, an anomalously positive land–sea thermal contrast is formed. An anomalous convergent zone in relation to the positive land–sea thermal contrast, located in the eastern part of the IIE, will favor the IIE to move more eastward than normal, and vice versa. An anomalous divergent zone located in the eastern part of the IIE will benefit the IIE to shift more westward than normal. Experiments using a linear baroclinic model confirm the physical processes revealed by the observational analysis.

✉ Jie Cao
caoj@ynu.edu.cn

[1] Meteorological Institute of Yunnan Province, Kunming, China

[2] Department of Atmospheric Sciences, Yunnan University, Kunming 650091, China

[3] Yunnan Key Laboratory of International Rivers and Transboundary Eco-Security, Kunming, China

[4] School of Environmental Science and Engineering, Sun Yat-sen University, Guangzhou, China

Keywords Indian–East Asian summer monsoon interface · Zonal movement · Land–sea thermal contrast · East Asia

1 Introduction

China is situated in the strongest monsoon area in the world—that of the Asian monsoon (Flohn 1957; Chang 2004; Wang 2006). The water vapor carried separately by the two subsystems of the Asian monsoon—the Indian summer monsoon (ISM) and East Asian summer monsoon (EASM)—mixes around their interface area (IIE), transports into East Asia, and further regulates the occurrence of flooding and droughts in summer over China (e.g., Lau and Li 1984; Tao and Chen 1987; Ding 1994; Zhang 2001; Zhou and Yu 2005; Wu et al. 2012a; Fig. 3 in this study). Based on previous researches on the IIE (e.g., Jin and Chen 1982; Wang and Lin 2002; Wang et al. 2003), Cao et al. (2012) objectively defined an IIE index and found that the zonal movement of IIE is closely related to regional rainfall anomalies in East Asia. When the IIE moves eastward, summer rainfall is significantly stronger than normal over the lower and middle reaches of the Yangtze River, and vice versa. Consequently, understanding the physical processes related to the IIE interannual variability may be valuable for the prediction of summer droughts and floods in East Asia, from the viewpoint of the interaction between the ISM and EASM.

The land–sea thermal contrast induced by the annual cycle of solar irradiation is a crucial driver of the Asian summer monsoon circulation (e.g., Meehl 1994; Webster et al. 1998; Chou 2003; Wu et al. 2012a). Large temperature increases are apparent from May to June over Eurasia, centered on the Tibetan Plateau, but no obvious temperature

change is found over the Indian Ocean (Li and Yanai 1996). Subsequently, the meridional temperature gradient south of 35°N is reversed and initiates the summer monsoon over the Indian subcontinent (Flohn 1957, 1960). The commencement of the summer monsoon over East Asia, Southeast Asia and the South China Sea is also closely associated with the land–sea thermal contrast, which directly impacts on the monsoon flows over these places (Ueda and Yasunari 1998; Zhao et al. 2007). Xu et al. (2010) suggested that the presence of a mid-latitude zonal land–sea distribution induces a strong zonal pressure gradient between the continent and ocean. The gradient in turn results in the formation of an East Asian subtropical monsoon. The thermal contrast between the Asian continent and the adjacent ocean is reinforced by the Tibetan Plateau, which acts as an elevated heat source, and further intensifies the summer monsoon (Duan and Wu 2005; Wu et al. 2007, 2009, 2012a, b; Liu et al. 2012; Duan et al. 2013; Tang et al. 2013; Wang et al. 2013).

The land–sea thermal contrast also influences the variability of the Asian summer monsoon. Meehl (1994) studied the impact of land surface temperature on the Asian summer monsoon with an atmospheric general circulation model, and suggested that greater land–sea temperature contrast (i.e., higher land temperatures), lower sea-level pressure over land, less snow cover, and greater soil moisture will induce stronger summer monsoons (defined as higher-averaged rainfall over south Asia). Fu and Fletcher (1985) found high correlation between Tibet–tropical ocean thermal contrast and Indian monsoon rainfall. Kucharski et al. (2011) found that north–south thermal contrast mainly contributes to surface atmospheric cyclones and precipitation over northern India. When Indian Ocean sea surface temperatures are normal, the east–west thermal gradient will result in a low-level cyclone and subsequent rainfall activity in the Bay of Bengal and southern India. Li and Yanai (1996) studied the interannual variability of the Asian summer monsoon associated with land–sea thermal contrast. They found that strong/weak Asian summer monsoon years are related to positive/negative tropospheric temperature anomalies over Eurasia but negative/positive sea surface temperature anomalies over the equatorial eastern Pacific, Arabian Sea, Bay of Bengal, and South China Sea. Wang and Qian (2009) suggested that land and sea thermal anomalies are closely related to the summer circulation, as well as Meiyu rainfall and South China Sea summer monsoon intensity. Kamae et al. (2014) pointed out that the land–sea surface air temperature contrast is closely coupled with anticyclonic anomalies around the Okhotsk Sea and the Philippines and an anomalous cyclone over Japan during a positive phase (warmer over land and colder over ocean) on the interannual time scale, and vice versa.

Previous studies have investigated the land–sea thermal contrast in the upper and lower troposphere in forcing the Asian summer monsoon (e.g., Li and Yanai 1996; Dai et al. 2013). They indicated that the land–sea thermal contrast in the upper troposphere is more dominant than that in the lower troposphere in driving the Asian summer monsoon and influencing its variations (Sun et al. 2010; Dai et al. 2013). The upper-tropospheric land–sea thermal contrast is larger than the lower-tropospheric, and its contribution to the strength of the Asian summer monsoon is around double (Dai et al. 2013). Yang et al. (2006) found that the latent heating released from the convection concentrates in the upper troposphere in the lower latitudes, suggesting that lower-latitude strong convection plays an important role in affecting the land–sea thermal contrast in the upper troposphere.

Although previous studies also pointed out that the variability of the Asian summer monsoon is affected by many other factors, such as the sea surface temperature and wave patterns in the mid-high latitudes (e.g., Chang 2004; Wang 2006; Ueda et al. 2009; Yoon and Yeh 2010 and reference therein), the fundamental effect of the land–sea thermal contrast in the establishment and variations of the Asian summer monsoon motivates us to explore the possible relationship between the land–sea thermal contrast and the interannual variation of the IIE. Specifically, this study attempts to answer the following questions: Is the land–sea thermal contrast related to the IIE variability? If so, what are the relative contributions, quantitatively, of the land and sea thermal anomalies over East Asia to the IIE variability? Furthermore, what are the physical processes involved?

The remainder of the paper is structured as follows. The datasets and methods used are described in Sect. 2. Section 3 investigates the relationship between the IIE and the adiabatic heating over East Asia, the circulation structure associated with the covariation of the land–sea thermal contrast and the IIE, the relative contribution of the land and sea thermal anomalies over East Asia to the IIE variability, and the possible mechanism through which the land–sea thermal contrast over East Asia relates to the variability of the IIE. Section 4 verifies the relationship revealed in Sect. 3 with a linear baroclinic model (LBM, Watanabe and Kimoto 2000). A summary and further discussion are provided in Sect. 5.

2 Data and method

We use twentieth century reanalysis data (Version 2), National Centers for Environmental Prediction–Department of Energy (NCEP–DOE) reanalysis II and outgoing longwave radiation (OLR) data provided by NOAA/OAR/ESRL PSD, and CPC merged analysis of precipitation (CMAP) over the period

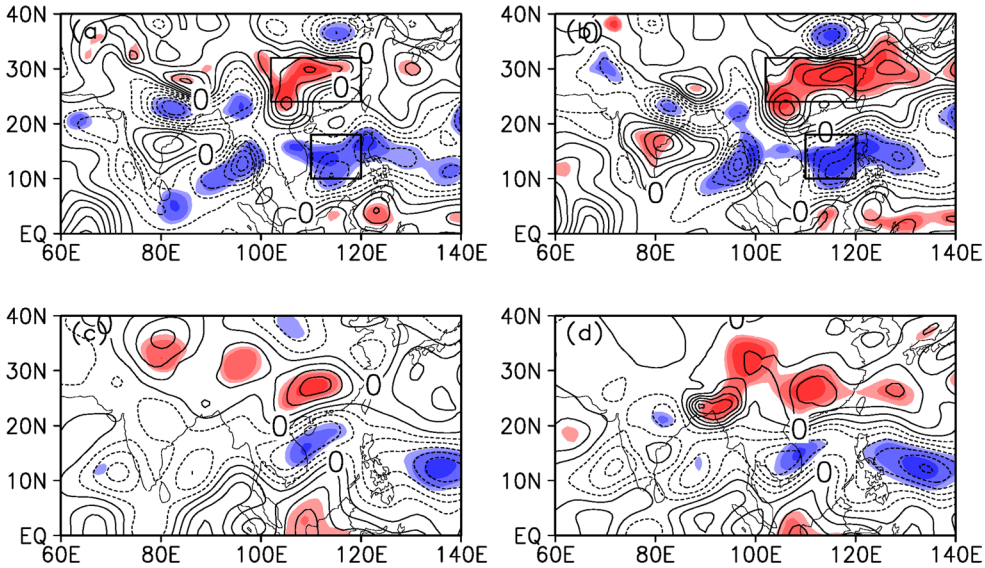

Fig. 1 The (**a**, **c**) apparent heating source and (**b**, **d**) apparent moisture sink regressed onto the IIE index, calculated based on (**a**, **b**) twentieth century reanalysis data (Version 2) and (**c**, **d**) NCEP–DOE reanalysis II data. The *areas shaded with blue* or *red* from *light* to *dark* denote correlation coefficients passing the significance test at the 90, 95 and 99 % confidence level, respectively. Contour intervals are 1.5 W m^{-2}

1979–2008 (Liebmann and Smith 1996; Xie and Arkin 1997; Kanamitsu et al. 2002; Compo et al. 2006, 2011; Whitaker et al., 2004). The resolution of the twentieth century reanalysis data (Version 2) is 2° in latitude and longitude, and there are 19 pressure levels from 1000 to 100 hPa. The resolution of the NCEP–DOE reanalysis II is 2.5° in latitude and longitude, and there are 12 pressure levels from 1000 to 100 hPa. The resolution of the OLR and gridded precipitation is 2.5° in latitude and longitude. Here, summer denotes June through August (JJA). The IIE is defined by the partial deviation of equivalent potential temperature with respect to longitude being equal to zero around 100°E (Cao et al. 2012). The apparent heat source, Q_1, and the apparent moisture sink, Q_2 (Yanai et al. 1973, 1992; Li and Yanai 1996), are estimated using the reanalysis data and the thermodynamic equation as follows:

$$Q_1 = C_p\left(\frac{p}{p_0}\right)^{\kappa}\left(\frac{\partial\theta}{\partial t} + \mathbf{v}\cdot\nabla\theta + \omega\frac{\partial\theta}{\partial p}\right), \tag{1}$$

$$Q_2 = -L\left(\frac{\partial q}{\partial t} + \mathbf{v}\cdot\nabla q + \omega\frac{\partial q}{\partial p}\right). \tag{2}$$

where θ is potential temperature; $\mathbf{v}$ is horizontal velocity; ω is vertical velocity at the isobaric surface; q is the mixing ratio of water vapor; t is time; p is pressure; C_p is the specific heat at constant pressure of dry air; $k = R/C_p$, where R is the gas constant of dry air and L is the latent heat of condensation; and ∇ is the isobaric gradient operator. The column-integrated apparent heat source and apparent moisture sink are obtained by integrating Eqs. (1) and (2) from 100 hPa to the surface pressure, p_s, i.e.,

$$\langle Q_1\rangle = \frac{1}{g}\int_{100}^{P_s} Q_1 dp, \tag{3}$$

$$\langle Q_2\rangle = \frac{1}{g}\int_{100}^{P_s} Q_2 dp. \tag{4}$$

3 Results

3.1 Relationship between the IIE and the summer apparent heat source and apparent moisture sink

To quantitatively measure the relationship between the IIE and the apparent heat source and apparent moisture sink, the IIE index provided by Cao et al. (2012) is also employed in this study. Figure 1 presents the summer regressed apparent heat source and apparent moisture sink on the IIE index. The apparent heat source distribution associated with the IIE shows a meridional quadripole pattern, with one positive anomaly south of 10°N and east of 100°E, another positive anomaly between 20°N and 35°N and east of 100°E, one negative anomaly between 10°N and 20°N, and another negative anomaly north of 35°N and east of 100°E. Note that two anomalous centers are most significant among the meridional quadripole pattern, in which the positive center is located over the East Asian continent south of 35°N, and the negative center over the South China Sea (SCS). This pattern indicates that, when there is stronger diabatic heating over southeastern East Asia, the IIE index is larger and the IIE's position is farther east than normal; whereas, the weaker the diabatic heating over the SCS, the larger the IIE index and the farther east than normal the position of the IIE. When the diabatic heating centers each change with opposite direction over the two regions, the IIE index is smaller and the IIE's position is farther west than normal (Fig. 1a). The apparent moisture sink distribution closely resembles the meridional

quadripole pattern associated with the apparent heat source but with larger areas passing the significance test at a higher confidence level (Fig. 1b). The significance test results suggest that the latent heating may play an important role in the IIE variability in the total diabatic heating. In addition, the apparent heat source distribution associated with the IIE shows another meridional quadripole pattern over the Indian subcontinent (Fig. 1a)—and the apparent moisture sink, which becomes more significant over the southeastern part of the Indian subcontinent, distributes in a similar pattern to the apparent heat source (Fig. 1b). These findings indicate that the diabatic heating over the Indian subcontinent also contributes to the IIE variability to some extent.

Figure 1c, d, calculated using NCEP–DOE reanalysis II, share similar patterns as Fig. 1a, b. Thereunto, the significant positive correlation over southeastern East Asia and the significant negative correlation over the SCS are coherent to a large degree, suggesting that the results calculated using twentieth century reanalysis data (Version 2) are highly reliable, at least over the key research domain in this study. The reason why the significant correlation area and correlation intensity associated with twentieth century reanalysis data (Version 2) are stronger than those associated with NCEP–DOE reanalysis II data is that the IIE time series is also obtained using twentieth century reanalysis data (Version 2). Because the corresponding correlation intensity and area between the IIE and the diabatic heating over the Indian subcontinent are obviously weaker and smaller than those over southeastern East Asia in the two reanalysis datasets (Fig. 1), the contribution of the diabatic heating over the Indian subcontinent to the IIE variability is relatively small [agreeing with the associated consequences in Cao et al. (2012)]. Therefore, we still focus our study on East Asia.

It is worthwhile noting that the two anomalous centers over southeastern East Asia and the SCS have opposite correlation signs. This perhaps implies that the land–sea thermal contrast is the key physical factor influencing the IIE variability. As such, two indices of land–sea thermal contrast are respectively defined by the apparent heat source and the apparent moisture sink averaged in (24°–32°N, 102°–120°E) minus that averaged in (10°–18°N, 110°–120°E). The two regions are illustrated by the boxes in Fig. 1. The two indices of land–sea thermal contrast are denoted as I_{Q_1} and I_{Q_2}. It is easy to obtain the normalized time series of the two land–sea thermal contrast indices (Fig. 2). Figure 2 shows that the three time series share a similar evolution tendency at the interannual time scale. The correlation coefficient between the IIE index and I_{Q_1}, achieving 0.58, is larger than the critical value (0.57) at the 99.9 % confidence level. The correlation analysis results indicate that, when the index of the land–sea thermal contrast is larger than normal, i.e., the land–sea thermal contrast is stronger, the IIE's position will be farther east than normal. On the contrary, when the index is smaller than normal, the land–sea thermal contrast is weaker and the IIE's position will be farther west than normal. If we calculate the correlation coefficient between the IIE index and I_{Q_2}, its value reaches 0.66. The relatively large correlation coefficient associated with the apparent moisture sink, agreeing with those shown in Fig. 1, also suggests that the land–sea thermal contrast caused by latent heating may couple with the interannual variability of the IIE via a more efficient route.

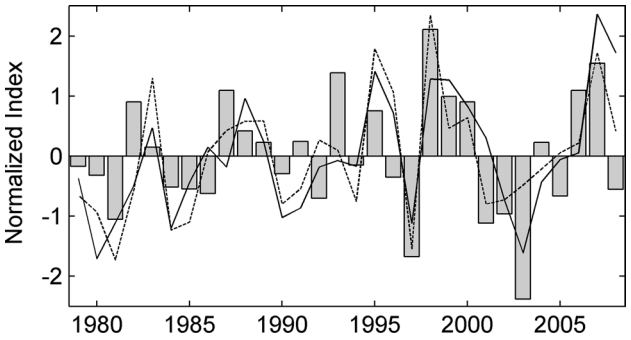

Fig. 2 The normalized land–sea thermal contrast index based on the apparent heating source (*solid line*); the normalized land–sea thermal contrast index based on the apparent moisture sink (*dashed line*); and the normalized IIE index (*bar chart*)

3.2 Circulation structure associated with the covariation of land–sea thermal contrast and the IIE

To investigate the atmospheric circulation structure associated with the covariation of land–sea thermal contrast and the IIE, we perform a composite analysis according to the normalized time series of the IIE and the land–sea thermal contrast with the diabatic heating (bar chart and the two lines in Fig. 2). Given the criterion that the I_{Q_1}, I_{Q_2} and the IIE index are all larger than 0.3 standard deviation, 6 out of 30 years can be identified as positive-anomaly years, in which the IIE shifts more eastward than normal. These years, hereafter referred to as EAY, are 1988, 1995, 1998, 1999, 2000 and 2007. According to the same criterion but with opposite sign, another 7 out of 30 years are chosen as negative-anomaly years, in which the IIE shifts more westward than normal. These years, hereafter referred to as WAY, are 1980, 1981, 1984, 1985, 1997, 2002 and 2003. Since the conditions in EAY mirror those in WAY to a large degree, the composite analysis is performed with the physical quantities in EAY minus those in WAY.

Figure 3a shows the diabatic heating and atmospheric circulation anomalies. In summer, the apparent heating source is significantly negative over the SCS, with

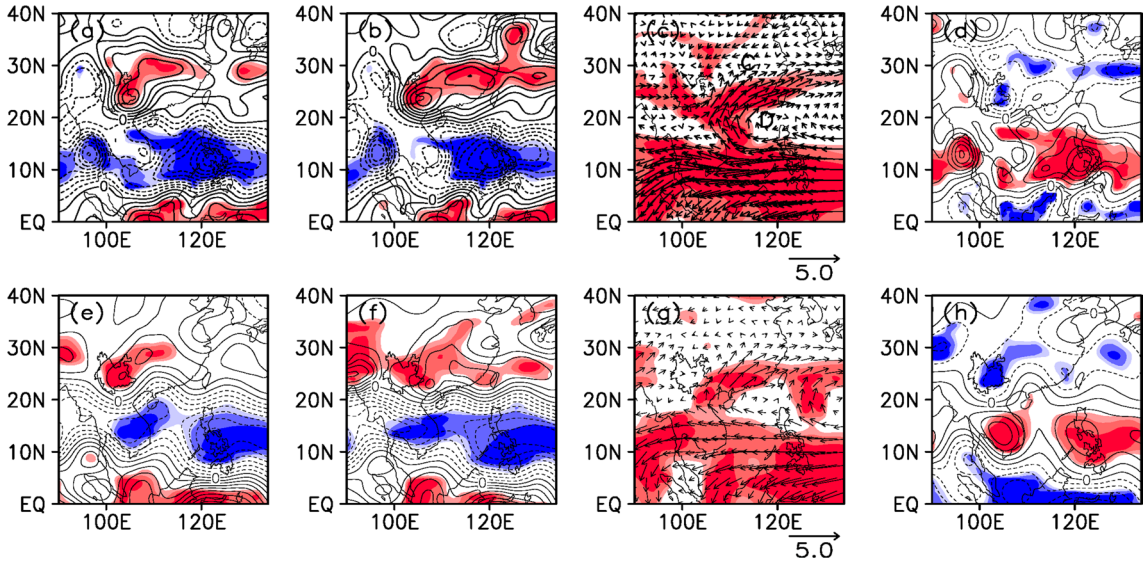

Fig. 3 Composite anomalies of summer (JJA) mean **a**, **e** apparent heating source (contour interval = 4 W m^{-2}), **b**, **f** apparent moisture sink (contour interval = 4 W m^{-2}), **c**, **g** horizontal winds at 850 hPa (units: m s^{-1}), and **d**, **h** vertical speed at 500 hPa (contour interval = 0.01 Pa s^{-1}) with EAY minus WAY. The results shown in panels **a**–**d** are calculated using twentieth century reanalysis data (Version 2), while **e**–**h** are calculated using NCEP–DOE reanalysis II data. *C* and *D* in **c** denote convergence and divergence. The *areas shaded with blue* or *red* from *light* to *dark* denote the differences passing the significance test at the 90, 95 and 99 % confidence level, respectively

maximum anomalies under −36 W/m^2. On the contrary, the apparent heating source in EAY is conspicuously higher than that in WAY over southeastern East Asia, with maximum anomalies exceeding 20 W/m^2. The anomalous composite pattern of the apparent moisture sink not only shares a similar pattern as the apparent heating source, but also has a larger center value (24 W/m^2) over southeastern East Asia (Fig. 3b). Both anomalous patterns in Fig. 3a, b present an anomalous thermal gradient pointing to sea. Figure 3c, g shows that, along the western flank of an anomalous anticyclonic circulation over the SCS, an enhanced southerly extends northeastward from sea to land. Accompanying the anomalous anticyclone, subsidence anomalies appear in the same region with a central vertical speed of about 0.05 Pa/s at 500 hPa. Meanwhile, an anomalous convergence zone at the earth's surface and an anomalous ascending air current at 500 hPa appear in southeastern East Asia. The ascending velocity is approximately −0.03 Pa/s. Figure 3e–h, calculated using NCEP–DOE reanalysis II data, reproduce the anomalous patterns in Fig. 3a–d, respectively. In accordance with Fig. 3, the significant OLR anomalies are negative over southeastern East Asia, and positive over the sea around the Philippines (Fig. 4a); whereas, the significant positive precipitation anomalies are located over southeastern East Asia, and significant negative anomalies are over the SCS (Fig. 4b). Note that the anomalous convergence zone is located just east of the IIE. Resulting from the combined thermodynamic and dynamic forcing in which

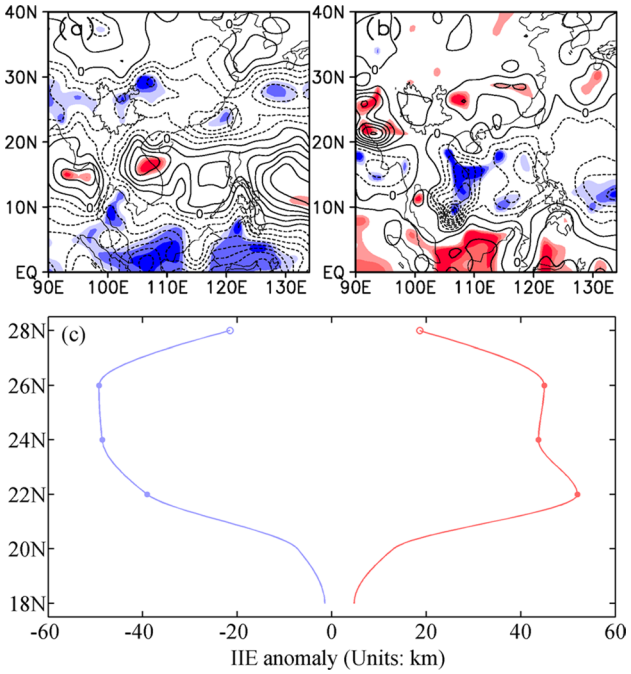

Fig. 4 Composite anomalies of summer (JJA) mean **a** OLR (contour interval = 2 W m^{-2}), **b** precipitation (contour interval = 1 mm d^{-1}), and **c** IIE with EAY minus normal (*red line*) and WAY minus normal (*blue line*). The *areas shaded with blue* or *red* from *light* to *dark* denote differences passing the significance test at the 90, 95 and 99 % confidence level, respectively. The *open* and *solid circles* in **c** denote the differences passing the significance test at the 95 and 99 % confidence level, respectively

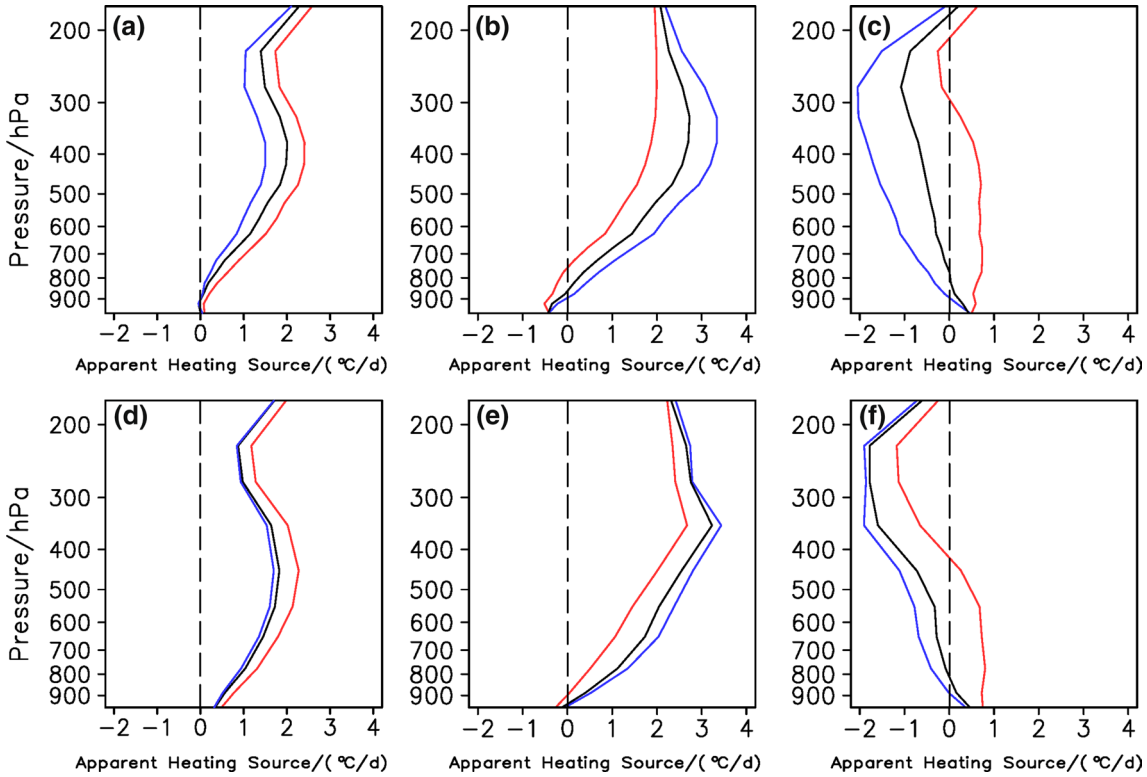

Fig. 5 Vertical profiles of the apparent heating source over **a**, **d** southern China (24°–32°N, 102°–120°E), **b**, **e** the South China Sea (10°–18°N, 110°–120°E), and **c**, **f** the difference between them. *Black line*—normal years; *red line*—EAY; *blue line*—WAY (units: °C day^{-1}). The results shown in panels **a**–**c** are calculated using twentieth century reanalysis data (Version 2), while **d**–**f** are calculated using NCEP–DOE reanalysis II data

the difference of I_{Q_1} and I_{Q_2} between EAY and WAY are 2.49 and 2.36, i.e., coupled with the anomalous convergence zone in particular, the IIE shifts more eastward in EAY, in which the displacement differences at 22°N, 24°N and 26°N pass the significance test at the 99 % confidence level, and that at 28°N passes the significance test at the 95 % confidence level (Fig. 4c). In fact, the difference of the IIE index runs up to 2.19, passing the significance test at the 99.9 % confidence level. The IIE moving more westward will happen under generally the opposite conditions of each physical quantity analyzed above.

To further obtain the vertical structure of diabatic heating associated with the covariation of land–sea thermal contrast and the IIE, we sequentially perform composite analyses of the vertical profiles of the apparent heating source and the apparent moisture sink. Figure 5 shows the vertical profile of the apparent heating source over southern China, the SCS, and the difference between them. The normal vertical distributions over southern China present large heating centered between 300 and 500 hPa. In EAY and WAY, the vertical profiles share the same pattern as in normal years. In EAY, the apparent heating source at layers above 925 hPa is larger than in normal years, whereas those above 800 hPa in WAY are less than in normal years over southern China (Fig. 5a). Figure 5b shows that the large heating over the SCS appears at layers above 500 hPa, and their values are generally larger than those over southern China. The apparent heating source in EAY is less than in normal years over the SCS at each isobaric surface, but larger in WAY than in normal years. The positive apparent heating source differences only appear below 300 hPa in EAY. The negative apparent heating source difference between southern China and the SCS appears from 200 to 800 hPa in WAY and normal years (Fig. 5c). Figure 5d–f, calculated using NCEP–DOE reanalysis II data, are almost the same as Fig. 5a–c, respectively. These results, which agree with those obtained by Dai et al. (2013) and Sun et al. (2010), suggest that the IIE variability correlates more closely to the upper tropospheric gradient of the apparent heating source over East Asia in comparison with the individual heating source over the SCS or southern China.

Figure 6 shows the vertical profile of the apparent moisture sink over southern China, the SCS, and the difference between them. The largest drying in normal years occupies the layer between 400 and 700 hPa over southern China. Also reflected in normal years, the vertical distributions of the apparent moisture sink show large drying centered

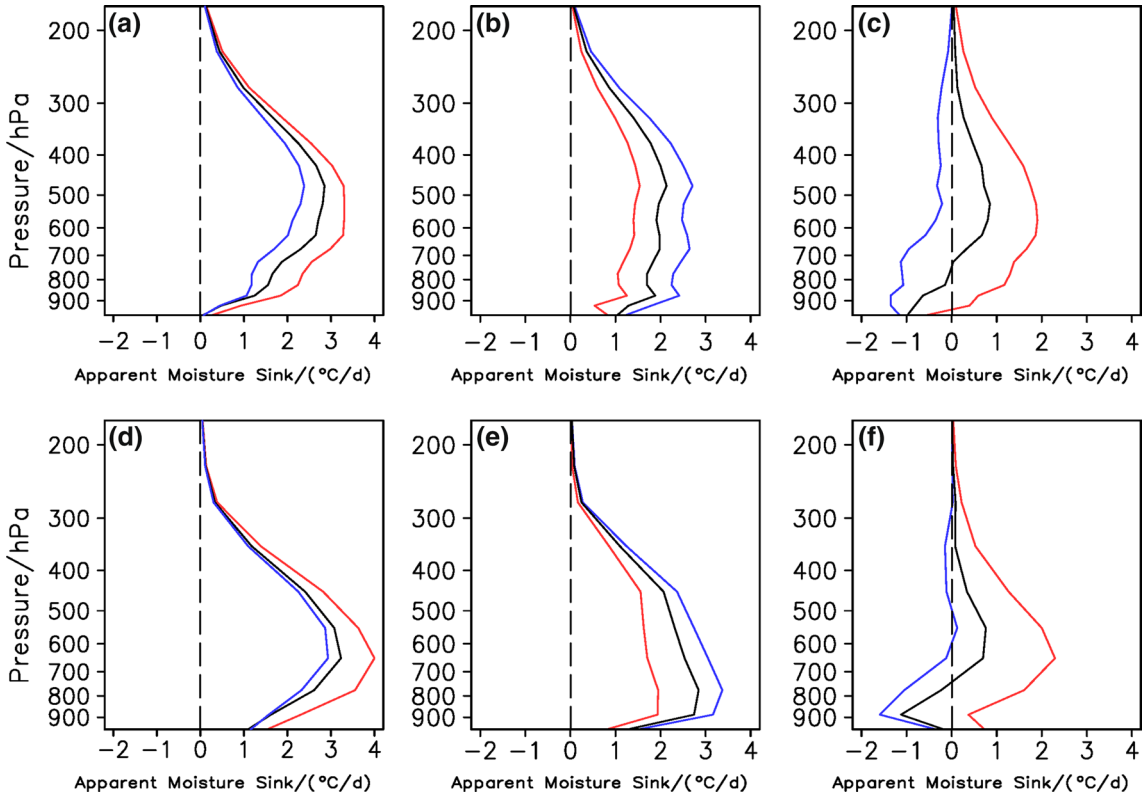

Fig. 6 As in Fig. 5 but for the apparent moisture sink (units: °C day^{-1})

between 400 and 700 hPa in EAY (WAY), and their values are greater (less) than in normal years at each layer (Fig. 6a). Figure 6b demonstrates that the relatively large apparent moisture sink over the SCS appears at layers between 400 and 800 hPa with a wavy pattern. The apparent moisture sink in EAY over the SCS is less than in normal years, but that in WAY is larger than in normal years at each layer. The apparent moisture sink differences are negative at each layer in WAY, positive at the layers above 1000 hPa in EAY, but negative below 700 hPa and positive above 700 hPa in normal years (Fig. 6c). Figure 6d–f, calculated using NCEP–DOE reanalysis II data, correspondingly show similar patterns as Fig. 6a–c. The results also suggest that the apparent moisture sink differences over East Asia, especially in the upper troposphere, are more closely associated with the IIE variability than the individual apparent moisture sinks over the SCS or southern China to some extent.

3.3 The relative contribution of land and sea diabatic heating to the IIE's variability

The significant correlation between I_{Q_1}, I_{Q_2} and the IIE indicates that the land–sea thermal contrast associated with both the apparent heating source and the apparent moisture sink is closely related to the IIE's variability. To further obtain the relative importance of land and sea diabatic heating, we perform a regression analysis in which the normalized IIE index is the dependent variable, and the four normalized inter-dependent variables include the apparent heating source averaged in (24°–32°N, 102–120°E), the apparent heating source averaged in (10°–18°N, 110–120°E), the apparent moisture sink averaged in (24°–32°N, 102°–120°E), and the apparent moisture sink averaged in (10°–18°N, 110°–120°E). Denoting the four inter-dependent variables as x_1, x_2, x_3 and x_4, we can establish the corresponding quadribasic regression model (Table 1). The multiple correlation coefficient of the model reaches 0.67 and passes the significance test at the 99 % confidence level. We can therefore analyze the relative contribution of each variable according to the regression model.

Table 1 The quadribasic regression coefficients of the IIE index

Inter-dependent variable	x_1	x_2	x_3	x_4
Regression coefficient	0.052	−0.125	0.441	−0.141
Variance contribution (%)	2.2	6.9	28.5	7.9

Table 1 shows that the regression coefficients associated with diabatic heating over southern China are positive, and

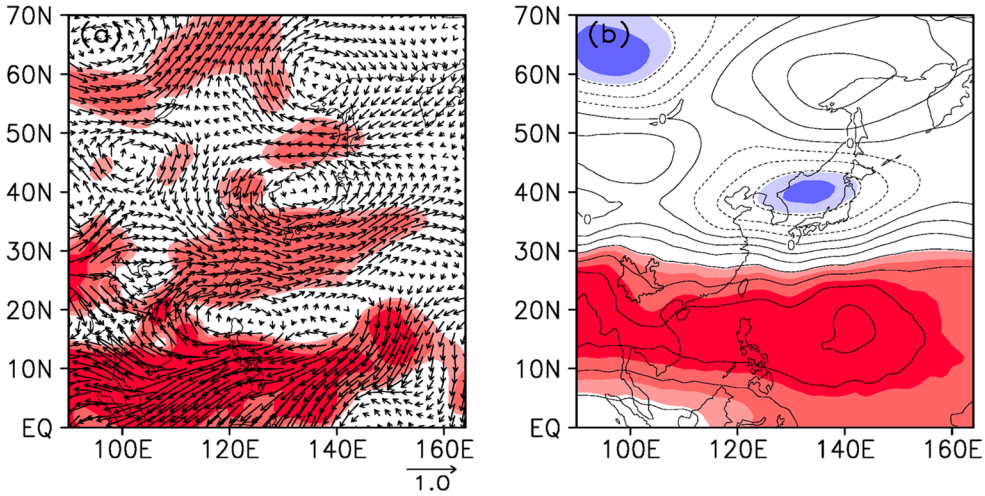

Fig. 7 Correlation coefficients between the **a** apparent moisture sink over southeastern East Asia and horizontal winds at 500 hPa and **b** the apparent moisture sink over southeastern East Asia and geopotential height at 500 hPa. The contour interval is 0.1 in **b**. The areas shaded from light to dark denote correlation coefficients passing the significance test at the 90, 95 and 99 % confidence level, respectively

those over the SCS have the opposite sign. This indicates the land–sea thermal contrast truly connects with the IIE's variability. The four factors explain 46.3 % of the total variance of the IIE index. Among them, the largest explained variance is 28.5 %, contributed by the inter-dependent variable x_3, and the explained variances of the remaining three inter-dependent variables almost have the same order. The correlation coefficient distribution at 500 hPa shows that the apparent moisture sink over southeastern East Asia clearly associates with the circulation from the lower latitudes region to the higher latitudes region. The higher apparent moisture sink over southern China is often accompanied by the intensification of southwesterly flow over the northwestern SCS, the southwestward extension and intensification of the western pacific subtropical high (WPSH), and the southward invasion of cold air (Fig. 7). The correlation coefficient of 0.57 shows that the apparent moisture sink over southern China is significantly and positively correlated to the zonal WPSH index developed by Lu (2002). These results indicate that the apparent moisture sink over southeastern East Asia is the most important factor in an anomalous land–sea thermal contrast, as land has a lower heat capacity than sea, and the apparent moisture sink over southern China links to the mid-high latitude circulation more strongly (Li and Yanai 1996; Wang and Qian 2009). It modulates the IIE's variability through the associated west–east movement of the WPSH (Cao et al. 2012).

3.4 Persistence of the correlation between the IIE and diabatic heating

To illustrate the persistence of the feature between the IIE, apparent heating source and apparent moisture sink, we show the temporal evolution of the correlation coefficient between the IIE and the 60 days running averaged apparent heating source along 114°E, as well as that between the IIE and the 60 days running averaged apparent moisture sink along 114°E (Fig. 8). The noticeable features are that the significantly positive correlation coefficients between diabatic heating and the IIE index occur around 30°N (land), the significantly negative correlation coefficients occur around 15°N (sea), and the correlation intensity connected with the apparent moisture sink is stronger in contrast to the apparent heating source. These two features agree with the results obtained above, and can be confirmed by the correlation maps associated with the 60 days running averaged index of land–sea thermal contrast and the IIE index (the black lines in Fig. 8b, d). Other new and conspicuous features are that the onset of significantly negative correlation between the IIE and the apparent moisture sink occurs mostly in early May over the SCS (Fig. 8c), and normally persists during the whole monsoon season, once it has established. The persistence is also obvious for the correlation between the IIE index and apparent heating source over the SCS (Fig. 8a). The significantly positive correlation over land begins in early summer, and ends in September. The correlation maps associated with the 90 days running averaged index of land–sea thermal contrast and the IIE index (the green lines in Fig. 8b, d) also reflect this persistence.

The persistence revealed above suggests that a positive feedback mechanism associated with the release of latent heating plays a critical role. The positive latent heating disturbance drives anomalous convergent low-level flow to the heating centers; the anomalous convergent low-level flow gathers more water vapor; the additional water vapor condenses to water through ascending movement; and, in turn, more latent heating is released, and vice versa (Charney and Eliassen 1964; Gill 1980; Zhang 1996; Wang et al. 2000). When a positive latent heating disturbance occurs in southeastern East Asia, and negative disturbance occurs in the SCS, a positive land–sea contrast is established (Fig. 3)

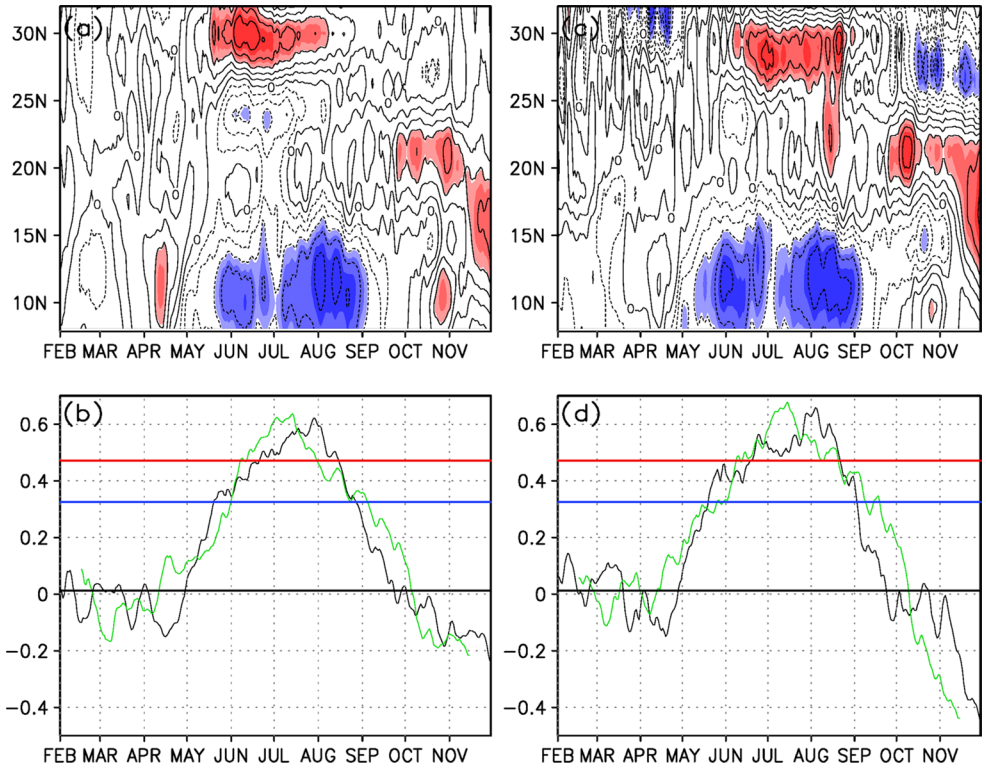

Fig. 8 Correlation coefficients between the 60 days running averaged apparent heating source along 114°E and the IIE index (**a**), correlation coefficients between the running averaged I_{Q_1} and the IIE index (**b**), correlation coefficients between the 60 days running averaged apparent moisture sink and the IIE (**c**), and correlation coefficients between the running averaged I_{Q_2} and the IIE (**d**). The *areas shaded blue* or *red* from *light* to *dark* denote correlation coefficients passing the significance test at the 90, 95 and 99 % confidence level, respectively. In **b**, **d**, the *thin black line* denotes correlation coefficients associated with the 60 days running averaged adiabatic heating, the *green line* denotes correlation coefficients associated with the 90 days running averaged adiabatic heating, the *thick blue line* denotes the critical value at the 90 % confidence level, and the *thick red line* denotes the critical value at the 99 % confidence level

and maintained during the whole summer monsoon season through the positive feedback mechanism (Fig. 8). The persistently positive land–sea contrast may induce a southwestward extension and intensification of the WPSH and a corresponding convergence zone over the north of the WPSH (Fig. 3e). The persistent convergence zone continuously attracts the IIE located at its western flank, and leads the IIE's position farther east than normal. In contrast, when a positive latent heating disturbance occurs in the SCS, and negative disturbance occurs in southeastern East Asia, a negative land–sea contrast is established (Fig. 4) and also preserved by the same positive feedback mechanism (Fig. 8). The WPSH related to the persistently negative land–sea contrast may continuously impel the IIE to move more westward than normal.

4 Model results

To qualitatively test the role of the thermal contrast over East Asia in impacting the local atmospheric circulation anomalies, we adopt an LBM with JJA climatology calculated from the NCEP–DOE reanalysis II. The apparent moisture sink patterns associated with the IIE variability in WAY, EAY and normal years serve as the prescribed forcing for the dry version LBM. We use a version with a horizontal resolution of T42 and 20 sigma levels in the vertical direction. In the LBM, the time scales of Rayleigh friction and Newtonian damping are 0.5 day^{-1} for $\sigma \geq 0.9$, 1 day^{-1} for $\sigma \leq 0.03$, and 20 day^{-1} for σ between 0.9 and 0.03. A detailed description of the LBM can be found in Watanabe and Kimoto (2000). Figure 9a shows the prescribed vertical profiles of the heating source in normal years and EAY, which are the same as the observed profiles of the apparent moisture sink shown in Fig. 6a, b, but in the sigma coordinate system. The center intensities of the heating sources are determined by the prescribed vertical profiles, and the corresponding spatial distributions exhibited in Fig. 9b, c are similar to those shown in Fig. 3.

To obtain the atmospheric response to the diabatic heating, we adopt a time integration method. Because the atmospheric circulation response is close to the steady state

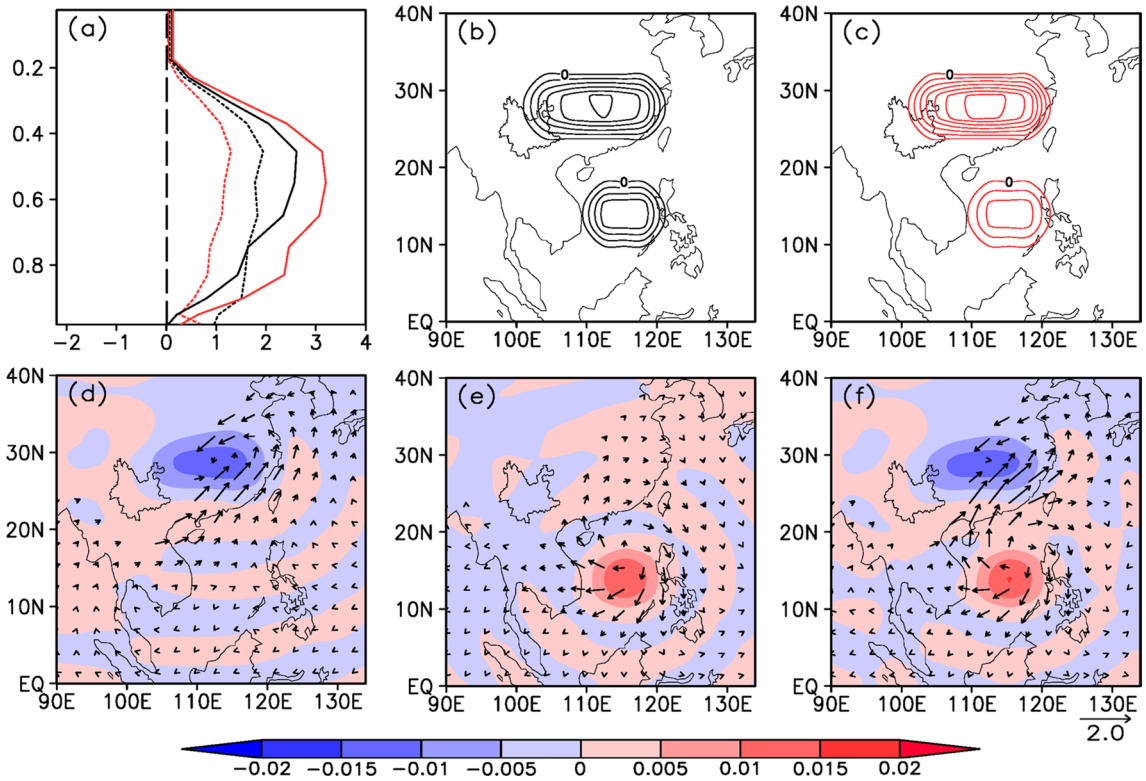

Fig. 9 Vertical profile (**a**) and horizontal distribution ($\sigma = 0.55$) of the prescribed heating source in normal years (**b**) and EAY (**c**). The contour interval is 0.5 K day^{-1} in **b**, **c**. Panels **d**–**f** show the horizontal wind anomalies (units: m s^{-1}) at 850 hPa and vertical velocity anomalies (units: Pa s^{-1}) at 500 hPa, forced by the heating source over southern China, the SCS, and both, respectively. In **a**, the *black solid line* denotes the vertical profile in normal years over southern China, the *red solid line* denotes the vertical profile in EAY over southern China, the *black dotted line* denotes the vertical profile in normal years over the SCS, the *red dotted line* denotes the vertical profile in EAY over SCS, and the *dashed line* denotes zero heating

after day 11, the differences between EAY and normal years at day 15 are shown as the steady response. Figure 9d shows the simulated horizontal wind and vertical velocity differences between EAY and normal years after only imposing the heating source in southern China. Because the intensity of the heating source in EAY is stronger than in normal years over southern China, the positive anomaly of the heating source will result in a cyclonic anomaly at 850 hPa, with ascending motion at 500 hPa around the same region. Stronger southwesterlies prevail over the southern flank of the cyclonic anomaly. A relatively weak anticyclonic anomaly, which may benefit the southwestward extension and intensification of the WPSH, is also forced out over the SCS. The circulation anomalies, responding to the heating source, resemble the composite anomalies of summer mean circulation (Fig. 3c, d, g, h). This implies the relative importance of the heating source over southern China in influencing the circulation responses associated with the IIE variability.

If the heating source is only imposed on the SCS, it can be seen from Fig. 9e that an anticyclonic anomaly at 850 hPa, with descending motion at 500 hPa, which will favor the southwestward extension and intensification of the WPSH, are centered on the negative anomaly of the heating source. However, the anomalous southwesterly is very weak over the northern flank of the anticyclonic anomaly. It is thus clear that the contribution of the heating source over the SCS to the circulation responses associated with the IIE variability is smaller than the contribution of the heating source over southern China. These results are consistent with those reported in Sect. 3.3.

If the heating sources are imposed on southern China and the SCS, we find that, at 850 hPa (Fig. 9f), a significant cyclonic anomaly dominates southern China and a significant anticyclonic anomaly controls the SCS. The ascending (descending) motion at 500 hPa matches well with the cyclonic (anticyclonic) anomaly over southern China (the SCS). In comparison with Fig. 9d, e, the circulation anomalies responding to the joint influences of the heating sources over southern China and the SCS (Fig. 9f) are the closest to the observational anomalies shown in Fig. 3c, d, g, h. These modeling results suggest that the land–sea thermal contrast, contributed by the apparent moisture sink, probably impels the IIE's movement

through significantly impacting the large-scale circulations, such as WPSH.

5 Summary and discussion

Based on atmospheric variables from the twentieth Century reanalysis (Version 2) and NCEP–DOE reanalysis II datasets, CMAP precipitation, OLR data and the IIE index, in this study we have calculated the apparent heating source and apparent moisture sink, and defined two land–sea contrast indices. According to the two land–sea contrast indices and IIE index, a significantly positive relationship between the diabatic heating and variability of the IIE index over East Asia has been identified by correlation analysis. The circulation structure associated with the covariation of land–sea thermal contrast and the IIE has been further revealed by composite analysis. The corresponding results obtained from diabatic heating and circulation using the two reanalysis datasets, OLR, and precipitation agree well, and therefore possess high reliability. During summers with positive indices, i.e., diabatic heating anomalies above (below) normal over southern China (the SCS), an anomalous thermal gradient pointing to the sea—that is, a positive index of land–sea thermal contrast—builds up, and low-level convergence (divergence) anomalies, accompanied by ascending (descending) motion, dominate over southeastern East Asia (the SCS). The anomalous convergence zone, with a lower-than-normal OLR and heavier-than-normal rainfall over southern China, attracts the IIE, located precisely at the western flank of the convergence zone, and leads to an eastward shift of the IIE. During summers with negative indices, i.e., diabatic heating anomalies below (above) normal over southern China (the SCS), the opposite condition occurs, inducing a westward movement of the IIE.

The north–south land–sea thermal contrast over East Asia is one of the crucial physical factors in relation to the zonal movement of the IIE during summer, in which the synchronous apparent moisture sink over southern China is the most important factor. The release of latent heating exerted by the low-frequency variability of anomalous land–sea thermal contrast is one of the most important physical processes because the vertical separation of peaks of the apparent heating source and apparent moisture sink is observed in WAY, EAY and normal years of diabatic heating and the IIE. Once the key physical process starts during the preceding period, it will exert significant control over the IIE's position during the whole summer monsoon season. The modeling results based on the LBM further substantiate the crucial physical process mentioned above.

Earlier studies suggested that there is a significant relationship between the zonal movement of the WPSH and convection over the tropical western Pacific. In particular, this can be caused by land–sea thermal contrast, which may relate directly to the zonal movement of the IIE. The zonal movement of the WPSH is closely related to convection over the tropical western Pacific, the East Asian subtropics, and the Indian summer monsoon region (Lu 2001; Lu and Dong 2001; Lu and Lin 2009; Zhou et al. 2009; Xie et al. 2009; Liu et al. 2012). In fact, the correlation coefficients between the zonal WPSH index, apparent moisture sink over SCS (−0.47), and apparent moisture sink over southern China (0.57) pass the significance test at the 99 % confidence level. The correlation coefficient (0.32) between the zonal WPSH index and apparent moisture sink averaged in the Indian monsoon region (14°–20°N, 78°–80°E) pass the significance test at the 90 % confidence level. These results are compatible with the present results (Figs. 3, 4), suggesting that the WPSH is one of the major circulation systems through whose zonal movement the land–sea thermal contrast, mainly contributed by the apparent moisture sink, connects with the west–east displacement of the IIE.

Huang and Li (1987) and Nitta (1987) found that a teleconnection pattern, commonly known as the East Asia/Pacific or Pacific–Japan teleconnection, appears from the area around the Philippines to North America, through East Asia, during boreal summer. This well-known teleconnection dominates the climatic variability over East Asia. They found that the heat source anomalies over the tropical western North Pacific greatly influence the activities of the teleconnection pattern by the propagations of quasi-stationary planetary waves. Above- (below-) normal convective activity over the tropical western North Pacific is associated with anticyclonic (cyclonic) anomalies over mid-latitude East Asia (Huang and Li 1987; Nitta 1987; Huang and Sun 1992). The anomalous circulation of the teleconnection pattern, in turn, can intensify the anomalous convective activity around the Philippines by enhancing evaporation and moisture convergence and dynamically leading anomalous vertical motion (Kosaka and Nakamura 2010). Figure 7 in this study shows an almost perfect East Asia/Pacific or Pacific–Japan teleconnection pattern, suggesting that the East Asia/Pacific or Pacific–Japan teleconnection may be the quasi-stationary planetary waves controlling the IIE's variability. So, the mechanism revealed by Kosaka and Nakamura (2010) also offers a successful interpretation of the persistence of the correlation between the IIE and diabatic heating (Fig. 8).

The East Asia/Pacific or Pacific–Japan teleconnection will also induce a well-known seesaw pattern of tropical–subtropical rainfall. The subtropical rainfall anomaly, closely associated with the diabatic heating anomaly, is implicitly presumed as a response to anomalous circulations, while the tropical rainfall anomaly or the diabatic heating anomaly is considered as one of the sources for

extratropical circulation anomalies (e.g., Nitta 1987; Huang and Sun 1992; Kosaka and Nakamura 2006, 2010). However, some studies have indicated that the subtropical rainfall anomaly or subtropical diabatic heating anomaly can also influence the larger-scale atmospheric circulation (e.g., Kodama 1999; Lu and Lin 2009; Matsumura et al. 2015). The results of the observational analysis and LBM model experiments in this study agree with the latter, suggesting that the diabatic heating anomaly over southern China can, to some extent, drive the zonal movement of the IIE.

The persistent correlation between the IIE and apparent moisture sink in the low-frequency band (60–90 days) suggests that the low-frequency apparent moisture sink appearing at the end of spring could be used as a potential predictor of IIE activity on the interannual time scale. Nevertheless, the forecast period of validity is relatively short. To increase the potential for extending the forecast, other factors impacting on the low-frequency apparent moisture sink, e.g., ENSO, and the thermal condition of the Indian Ocean and Tibetan Plateau, which significantly influences East Asian climates (e.g., Wang et al. 2000; Ding and Chan 2005; Lu and Ren 2005; Ueda et al. 2009; Xie et al. 2009; Huang et al. 2012), should be considered. These are also interesting issues and deserve further study in the future.

Acknowledgments We thank Prof. M. Watanabe for providing the linear baroclinic model and the anonymous reviewers for their valuable comments that lead to improvement of the manuscript. This work was supported by the National Natural Science Foundation of China (41375097 and 41375091) and the Jiangsu Collaborative Innovation Center for Climate Change.

References

Cao J, Hu J, Tao Y (2012) An index for the interface between the Indian summer monsoon and the East Asian summer monsoon. J Geophys Res Atmos 117:D18108. doi:10.1029/2012jd017841

Chang CP (2004) East Asian monsoon, vol 2. World Scientific, Singapore

Charney JG, Eliassen A (1964) On the growth of the hurricane depression. J Atmos Sci 21:68–75

Chou C (2003) Land–sea heating contrast in an idealized Asian summer monsoon. Clim Dyn 21:11–25

Compo GP, Whitaker JS, Sardeshmukh PD (2006) Feasibility of a 100-year reanalysis using only surface pressure data. Bull Am Meteorol Soc 87:175–190

Compo GP, Whitaker JS, Sardeshmukh PD, Matsui N, Allan R, Yin X, Gleason B, Vose R, Rutledge G, Bessemoulin P (2011) The twentieth century reanalysis project. Q J Roy Meteorol Soc 137:1–28

Dai A, Li H, Sun Y, Hong LC, Chou C, Zhou T (2013) The relative roles of upper and lower tropospheric thermal contrasts and tropical influences in driving Asian summer monsoons. J Geophys Res Atmos 118:7024–7045

Ding YH (1994) Monsoons over China, vol 16. Springer, Berlin

Ding YH, Chan JC (2005) The East Asian summer monsoon: an overview. Meteorol Atmos Phys 89:117–142

Duan A, Wu G (2005) Role of the Tibetan Plateau thermal forcing in the summer climate patterns over subtropical Asia. Clim Dyn 24:793–807

Duan A, Wang M, Lei Y, Cui Y (2013) Trends in summer rainfall over China associated with the Tibetan Plateau sensible heat source during 1980–2008. J Clim 26:261–275

Flohn H (1957) Large-scale aspects of the "summer monsoon" in south and east Asia. J Meteorol Soc Jpn 75:180–186

Flohn H (1960) Recent investigations on the mechanism of the "summer monsoon" of southern and eastern Asia. In: Proceedings of symposium on monsoon of the world, pp 75–88

Fu C, Fletcher JO (1985) The relationship between Tibet-tropical ocean thermal contrast and interannual variability of Indian monsoon rainfall. J Clim Appl Meteorol 24:841–847

Gill AE (1980) Some simple solutions for heat-induced tropical circulation. Q J Roy Meteorol Soc 106:447–462

Huang R, Li W (1987) Influence of the heat source anomaly over the tropical western Pacific on the subtropical high over East Asia. In: Proceedings of international conference on the general circulation of East Asia, Chengdu, pp 40–51

Huang R, Sun F (1992) Impacts of the tropical western Pacific on the East Asian summer monsoon. J Meteorol Soc Jpn 70:243–256

Huang R, Chen JL, Wang L, Lin ZD (2012) Characteristics, processes, and causes of the spatio-temporal variabilities of the East Asian monsoon system. Adv Atmos Sci 29:910–942

Jin ZH, and Chen LX (1982) On the medium-range oscillation of the East Asian monsoon circulation system and its relation with the Indian monsoon system. In: The national symposium collections on the tropical summer monsoon (in Chinese), People's Press of Yunnan Province, Kunming, pp 204–215

Kamae Y, Watanabe M, Kimoto M, Shiogama H (2014) Summertime land–sea thermal contrast and atmospheric circulation over East Asia in a warming climate—part I: past changes and future projections. Clim Dyn 43:1–16

Kanamitsu M, Ebisuzaki W, Woollen J, Yang S-K, Hnilo JJ, Fiorino M, Potter GL (2002) NCEP–DOE AMIP-II reanalysis (R-2). Bull Am Meteorol Soc 83:1631–1643

Kodama YM (1999) Roles of the atmospheric heating source in maintaining the subtropical convergence zones: an aqua-planet GCM study. J Atmos Sci 56:4032–4049

Kosaka Y, Nakamura H (2006) Structure and dynamics of the summertime Pacific–Japan (PJ) teleconnection pattern. Q J R Meteorol Soc 132:2009–2030

Kosaka Y, Nakamura H (2010) Mechanisms of meridional teleconnection observed between a summer monsoon system and a subtropical anticyclone. Part I: the Pacific–Japan pattern. J Clim 23:5085–5108

Kucharski F, Bracco A, Barimalala R, Yoo JH (2011) Contribution of the east–west thermal heating contrast to the South Asian monsoon and consequences for its variability. Clim Dyn 37:721–735

Lau K-M, Li M-T (1984) The monsoon of East Asia and its global associations—a survey. Bull Am Meteorol Soc 65:114–125

Li C, Yanai M (1996) The onset and interannual variability of the Asian summer monsoon in relation to land–sea thermal contrast. J Clim 9:358–375

Liebmann B, Smith CA (1996) Description of a complete (interpolated) outgoing longwave radiation dataset. Bull Am Meteorol Soc 77:1275–1277

Liu Y, Wu G, Hong J, Dong B, Duan A, Bao Q, Zhou L (2012) Revisiting Asian monsoon formation and change associated with Tibetan Plateau forcing: II. Change. Clim Dyn 39:1183–1195

Lu R (2001) Interannual variability of the summertime North Pacific subtropical high and its relation to atmospheric convection over the warm pool. J Meteorol Soc Jpn 79:771–783

Lu R (2002) Indices of the summertime western North Pacific subtropical high. Adv Atmos Sci 19:1004–1028

Lu R, Dong B (2001) Westward extension of North Pacific subtropical high in summer. J Meteorol Soc Jpn 79:1229–1241
Lu R, Lin Z (2009) Role of subtropical precipitation anomalies in maintaining the summertime meridional teleconnection over the western North Pacific and East Asia. J Clim 22:2058–2072
Lu R, Ren B (2005) The influence of ENSO on the seasonal convection evolution and the phase of 30–60-day oscillations during boreal summer. J Meteorol Soc Jpn 83:1025–1040
Matsumura S, Sugimoto S, Sato T (2015) Recent intensification of the western Pacific subtropical high associated with East Asian summer monsoon. J Clim 28:2873–2883
Meehl GA (1994) Influence of the land surface in the Asian summer monsoon: external conditions versus internal feedbacks. J Clim 7:1033–1049
Nitta T (1987) Convective activities in the tropical western Pacific and their impact on the Northern Hemisphere summer circulation. J Meteorol Soc Jpn 65:373–390
Sun Y, Ding Y, Dai A (2010) Changing links between South Asian summer monsoon circulation and tropospheric land–sea thermal contrasts under a warming scenario. Geophys Res Lett. doi:10.1029/2009GL041662
Tang H, Micheels A, Eronen JT, Ahrens B, Fortelius M (2013) Asynchronous responses of East Asian and Indian summer monsoons to mountain uplift shown by regional climate modelling experiments. Clim Dyn 40:1531–1549
Tao SY, Chen LX (1987) A review of recent research on the EASM in China. Oxford University Press, Oxford, pp 60–92
Ueda H, Yasunari T (1998) Role of warming over the Tibetan Platean in early onset of the summer monsoon over the bay of Bengal and the South China Sea. J Meteorol Soc Jpn 76:1–12
Ueda H, Ohba M, Xie S-P (2009) Important Factors for the development of the Asian–Northwest Pacific summer monsoon. J Clim 22:649–669
Wang B (2006) The Asian monsoon. Springer, Berlin
Wang B, Lin H (2002) Rainy season of the Asian–Pacific summer monsoon. J Clim 15:386–398
Wang Z, Qian Y (2009) The relationship of land–ocean thermal anomaly difference with mei-yu and South China Sea summer monsoon. Adv Atmos Sci 26:169–179
Wang B, Wu R, Fu X (2000) Pacific–East Asian teleconnection: how does ENSO affect East Asian climate? J Clim 13:1517–1536
Wang B, Steven CC, Liu P (2003) Contrasting the Indian and East Asian monsoons: implications on geologic timescales. Mar Geol 201:5–21
Wang Z, Duan A, Wu G (2013) Time-lagged impact of spring sensible heat over the Tibetan Plateau on the summer rainfall anomaly in East China: case studies using the WRF model. Clim Dyn 42:1–14
Watanabe M, Kimoto M (2000) Atmosphere–ocean thermal coupling in the North Atlantic: a positive feedback. Q J R Meteorol Soc 126:3343–3369
Webster PJ, Magana VO, Palmer TN, Shukla J, Tomas RA, Yanai M, Yasunari T (1998) Monsoons: processes, predictability, and the prospects for prediction. J Geophys Res Oceans (1978–2012) 103:14451–14510
Whitaker JS, Compo GP, Wel X, Hamill TM (2004) Reanalysis without radiosondes using ensemble data assimilation. Mon Weather Rev 132:1190–1200
Wu G, Liu Y, Wang T, Wan R, Liu X, Li W, Wang Z, Zhang Q, Duan A, Liang X (2007) The influence of mechanical and thermal forcing by the Tibetan Plateau on Asian climate. J Hydrometeorol 8:770–789
Wu G, Liu Y, Zhu X, Li W, Ren R, Duan A, Liang X (2009) Multiscale forcing and the formation of subtropical desert and monsoon. Annal Geophys Atmos Hydros Space Sci 27:3631–3644
Wu G, Liu Y, Dong B, Liang X, Duan A, Bao Q, Yu J (2012a) Revisiting Asian monsoon formation and change associated with Tibetan Plateau forcing: I. Formation. Clim Dyn 39:1169–1181
Wu G, Liu Y, He B, Bao Q, Duan A, Jin F-F (2012b) Thermal controls on the Asian summer monsoon. Sci Rep 2:404
Xie P, Arkin PA (1997) Global precipitation: a 17-year monthly analysis based on gauge observations, satellite estimates, and numerical model outputs. Bull Am Meteorol Soc 78:2539–2558
Xie S-P, Hu K, Hafner J, Tokinaga H, Du Y, Huang G, Sampe T (2009) Indian Ocean capacitor effect on Indo-western Pacific climate during the summer following El Niño. J Clim 22:730–747
Xu Z, Qian Y, Fu C (2010) The role of land–sea distribution and orography in the asian monsoon. Part I: land–sea distribution. Adv Atmos Sci 27:403–420
Yanai M, Esbensen S, Chu J-H (1973) Determination of bulk properties of tropical cloud clusters from large-scale heat and moisture budgets. J Atmos Sci 30:611–627
Yanai M, Li C, Song Z (1992) Seasonal heating of the Tibetan Plateau and its effects on the evolution of the Asian summer monsoon. J Meteorol Soc Jpn 70:319–351
Yang S, Olson WS, Wang J-J, Bell TL, Smith EA, Kummerow CD (2006) Precipitation and latent heating distributions from satellite passive microwave radiometry. Part II: evaluation of estimates using independent data. J Appl Meteorol Clim 45:721–739
Yoon J, Yeh S-W (2010) Influence of the Pacific decadal oscillation on the relationship between El Niño and the northeast Asian summer monsoon. J Clim 23:4525–4537
Zhang M (1996) Impact of the convection-wind-evaporation feedback on surface climate simulation in general circulation models. Clim Dyn 12:299–312
Zhang RH (2001) Relations of water vapor transport from Indian monsoon with that over East Asia and the summer rainfall in China. Adv Atmos Sci 18:1005–1017
Zhao P, Zhang R, Liu J, Zhou X, He J (2007) Onset of southwesterly wind over eastern China and associated atmospheric circulation and rainfall. Clim Dyn 28:797–811
Zhou TJ, Yu RC (2005) Atmospheric water vapor transport associated with typical anomalous summer rainfall patterns in China. J Geophys Res Atmos 110:D08104. doi:10.1029/2004JD005413
Zhou T, Yu R, Zhang J, Drange H, Cassou C, Deser C, Hodson DL, Sanchez-Gomez E, Li J, Keenlyside N (2009) Why the western Pacific subtropical high has extended westward since the late 1970s. J Clim 22:2199–2215